Nonlinear Rayleigh-Taylor Evolution of a Three-Dimensional Multimode Perturbation

M. M. Marinak, S. G. Glendinning, R. J. Wallace, B. A. Remington, K. S. Budil, S. W. Haan, R. E. Tipton, and J. D. Kilkenny

Lawrence Livermore National Laboratory, Livermore, California 94551

(Received 18 December 1997)

The ablation front Rayleigh-Taylor evolution of a well-characterized 3D multimode surface perturbation was measured on a foil accelerated with an x-ray drive as it progressed into the weakly nonlinear regime. The perturbation pattern was locally random and consisted of modes within the first ten harmonics of a 300 μm square. The pattern evolved into bubbles separated by narrow, interconnecting spike sheets, unambiguously indicating entry into the nonlinear regime. Nonlinear effects occurred when mode amplitudes were relatively small: $\eta_n \ll \lambda_n/10$. Experimental results are in quantitative agreement with results of our numerical simulations. [S0031-9007(98)06073-6]

PACS numbers: 52.35.Py, 47.40.–x, 52.65.Kj, 52.70.La

In order to ignite successfully an imploding inertial confinement fusion (ICF) capsule the growth of perturbations due to hydrodynamic instabilities must be kept within acceptable levels. If perturbations attain sufficiently large amplitudes, excessive mixing of material from the capsule shell into the core will degrade implosion performance [1–3]. In targets driven by x rays from a hohlraum the hydrodynamic instabilities are usually seeded principally by perturbations on the material surfaces. For ignition capsules, such as those designed for the National Ignition Facility (NIF), the Rayleigh-Taylor (RT) instability [1,4] is responsible for most of the growth of the perturbations. With the best attainable surface finishes the RT growth of these perturbations progresses into the weakly nonlinear regime. There the amplitudes and shapes of these evolving features are determined by the nonlinear interactions between a broad spectrum of modes. Accurate modeling of nonlinear mode coupling and saturation of the hydrodynamic instabilities is therefore vitally important in predicting the performance of these ignition capsules.

Our past work with planar foils studied the growth of designated single mode and 2D multimode perturbations into the nonlinear regime [5–9]. Simulations of 2D modes reproduced the variation in perturbation growth with wavelength as well as various effects resulting from 2D mode coupling. One important reason for investigating the behavior of 3D perturbations is that the nonlinear saturation amplitude and growth rate of a mode depends upon its 3D perturbation shape. Simulations of 3D RT growth at a classical interface in Cartesian geometry [10,11], cylindrical converging geometry [11], and spherical converging geometry [12,13], as well as on foils driven directly by laser light [14,15], showed that the most round 3D perturbation shapes achieved the highest nonlinear growth. A potential flow model of bubbles on a classical interface [16], which extends the work of Layzer [17], also predicts that the most symmetric mode begins to saturate at the largest amplitude. Experimental measurements of x-ray driven foils on Nova which compared the evolution of a variety of pure modes having different shapes but the same wave number demonstrated this effect, in agreement with simulations [18].

Ultimately we are interested in predicting the evolution of a full spectrum of 3D modes growing simultaneously and interacting through mode coupling. A previous experiment studied the evolution of a foil driven directly by laser light in which modulations in the illumination pattern seeded perturbations [19]. Previously we reported preliminary, semiquantitative experimental results of growth on a randomly roughened surface, generated by sandblasting a glass mold [7]. We report here the first experimental measurements, accompanied by simulations, of the evolution of a designated, well-characterized 3D multimode surface perturbation on an ablatively driven foil. Since the hohlraum x-ray drive is essentially uniform over the foil, this experiment isolates the effect of the surface roughness. The surface perturbation consists of a spectrum of modes which includes those most dangerous for our ignition capsules. Instabilities seeded by this perturbation evolve from the linear regime to a degree of nonlinearity which is relevant for indirectly driven ignition capsules.

In the experiment surface perturbations are molded onto one side of a CH(Br) foil [$C_{50}H_{47}Br_{2.7}$] 62 μm thick, $\rho = 1.26$ g/cm^3, which is mounted across a 750 μm diameter hole in the wall of a 3000 μm long, 1600 μm diameter gold cylindrical hohlraum with the perturbations facing inward [9]. The foil is illuminated from the back by a 600 μm diameter source of x rays created by irradiating a disk of scandium with two Nova beams [20] delivering 3.2 kJ/beam in a 2 ns square pulse. Perturbations on the foil modulate the transmitted backlighter flux according to

$$I(x, y, t) = I_o(x, y, t)e^{-\int \kappa\rho\, dz},$$

where κ is the opacity. Measurements of the transmitted backlighter intensity determine modulations of optical

 0031-9007/98/80(20)/4426(4)$15.00

depth and therefore the amplitude of the areal density of the perturbation. The flexible x-ray pinhole imager (FXI) [21] was used to obtain gated images. Its resolution for these experiments was characterized earlier [18].

Eight $\lambda = 0.351$ μm, 2.5 kJ shaped Nova beams irradiate the hohlraum with a low intensity $\sim$1.0 ns foot followed by a rapid increase to peak power which is maintained over the interval 2.5–4.4 nsec, with the ratio of peak to foot laser power being $\sim$5. This new x-ray drive, which has been measured with the Dante x-ray diode array [22], creates a period of nearly uniform acceleration lasting $\sim$1.5 ns. The drive model employed in the simulations was obtained from a LASNEX [23] gold hohlraum simulation, with the amplitude renormalized to match the Dante measurement, corrected for the albedo of the hohlraum wall. This drive model reproduced well the measurement of the shock breakout trajectory through an aluminum wedge mounted on a hohlraum as viewed by a streaked uv imager [24] and measurement of the position of the back side of the foil using streaked side-on radiography [6,7,9]. Simulated conditions at the ablation front resembled those described for previous CHBr experiments [8]. In one of these experiments measurements of a flat CHBr foil in the same experimental geometry used here showed modulations induced by drive asymmetry were too small to measure [7].

Simulations of the ablatively driven foils were performed using the 3D radiation hydrodynamics code HYDRA [25]. These simulations employed STA opacities [26] with multigroup diffusion, and a Kevlar [$C_{14}H_{10}N_2O_2$ ($\rho = 1.26$ g/cm^3)] equation of state table [27]. To test further the components of our model we simulated foils having a variety of 2D single mode perturbations accelerated in Nova experiments utilizing this new drive. These had perturbation wavelengths of 30, 50, and 100 μm, initial amplitudes between 0.5–1.0 μm, and foil thicknesses of $\sim$60 μm. As seen in Fig. 1 the results showed good agreement with the time evolution of the Fourier modes of ln(exposure) measured in the experiments, as was the case for previous experiments performed with similar targets using a different drive [8]. For foils 62 μm thick simulations of small amplitude perturbations, which remained linear, predicted growth factors which peaked at wavelength $\lambda = 50$ μm, at a value of 50 at the end of 6.0 ns.

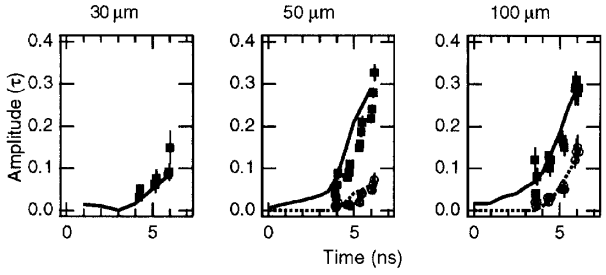

FIG. 1. Fourier components of ln(exposure) vs time for wavelengths of 30, 50, and 100 μm. The closed (open) symbols are the fundamental mode (second harmonic) obtained from radiographs. The solid (dashed) curves are the fundamental mode (second harmonic) from simulations.

The mold used to create the multimode perturbation was itself formed by laser ablation of 400 Gaussian-shaped pits [28] within each 300 μm square on the target. The perturbation was designed so that these pits overlap, creating a locally random, isotropic perturbation, shown in Fig. 2(a), which spans nearly a decade in Fourier space. Since weakly nonlinear mode coupling occurs over a bubble width, the short length scale random variation in the perturbation sets conditions for bubble formation and saturation. Over the largest transverse length scales of the system, the pattern possesses reflection symmetry; each 150 μm square is symmetric about its boundaries. The length scale of the reflection symmetry is too long for the lowest modes to determine weakly nonlinear saturation of the bubbles. The pattern is continued on the foil for an extra $\frac{1}{2}$ period beyond the 300 μm square, which defines the fundamental wavelength. This enables rigorous treatment of the boundary conditions in the code simulation. The perturbation placed on the foil was measured with a contact radiograph [9]. Details of this measurement will be described elsewhere. This specified surface perturbation, initialized in the simulation, consists of modes of

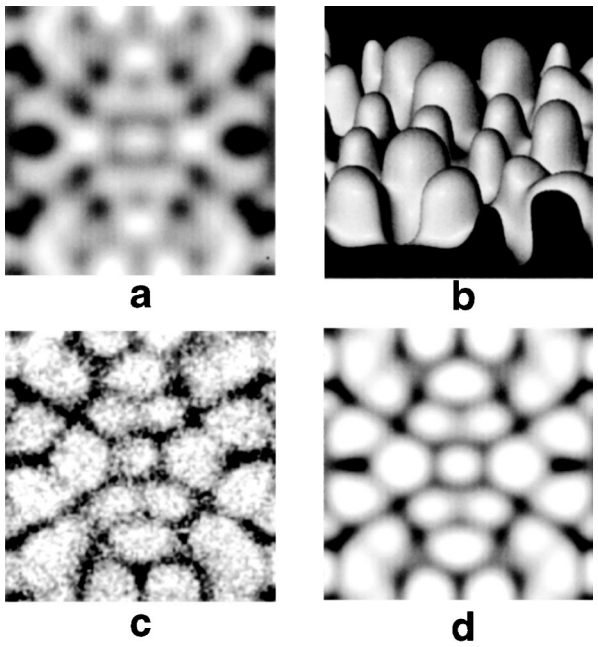

FIG. 2. (a) Contours of the designated initial multimode pattern shown on a 300 μm square. Darkest regions correspond to greatest foil thickness. (b) Density isocontour of 0.2 g/cm^3 from the HYDRA simulation at 6.0 ns. Perspective shows bubbles rising in the ablation front. (c) Experimental radiograph of the foil at 6.0 ns. The spikes appear dark in the radiograph. (d) Simulated radiograph at 6.0 ns, which includes the effect of instrumental resolution. Gray scales for (c) and (d) cover the same change in optical depth.

the form $\cos(k_x x)\cos(k_y y)$, where $(k_x, k_y) = 2\pi(m, n)/L$ with $(m, n) = (0{-}12, 0{-}12)$. A total of 168 modes was initialized with amplitudes obtained from the specified initial pattern, scaled to match the total measured 0.66 μm rms obtained from the radiograph.

The simulation of the multimode foil was performed over the 150 μm square section using a grid measuring $120 \times 120 \times 171$ zones, with reflection boundary conditions at the transverse boundaries. In the simulation the first shock breaks out at 2.2 ns. After a period of substantial linear regime RT growth the formation of broad bubbles becomes apparent in the simulation near 4.0 ns, indicating entry into the nonlinear regime. The perturbations become visible in the experimental radiographs during the period of measurement between 4.0 and 6.0 ns. Figure 2(c) shows an image in ln(exposure) of the multimode foil obtained with face-on radiography 6.0 ns. Under the influence of mode coupling, the pattern has evolved into broad bubbles in close packing surrounded by narrow, interconnecting spike sheets with local spike maxima occurring at the intersection of two or more sheets. Yet the structures in Fig. 2(c) retain a correspondence to the initial pattern. The average diameter of the bubbles at 6 ns is $\sim$50 μm, corresponding to the wavelength at the peak of the growth factor spectrum. The simulated radiograph from the HYDRA calculation at 6.0 ns is shown in Fig. 2(d). The comparison shows qualitatively the simulation reproduces well the details of the shapes and relative amplitudes of the various bubble-spike structures. A quantitative comparison of mode amplitudes is given below. The very short scale speckles in the experimental radiograph are instrumental noise.

The topology of the bubbles rising during the nonlinear phase is illustrated in Fig. 2(b), which shows a density isocontour in the ablation front from the HYDRA simulation at 6.0 ns. The tendency for the bubbles to assume the closest possible packing was observed in previous simulations of 3D multimode perturbations on foils [19,29,30] as well as on a classical interface [31]. A measure of the change in shape of the features is illustrated in Fig. 3, which shows the fraction of the simulated foil area having areal density within the lowest 20% of the range. The locations of lowest areal density correspond to the tops of the bubbles. The rapid rise in this fraction at 4 ns signals the onset of bubble formation in the mode coupling regime. Subsequent broadening of these bubbles is recorded in the continuing rise. Second-order mode coupling theory [32] was applied, using results from a set of linear growth factor calculations, and also predicts that broadening of bubbles should start to become noticeable at 4.0 ns.

The quantitative comparison of the Fourier spectra of the data with values obtained from the simulated radiograph is shown in Fig. 4(a). The evolution of the spectrum is well matched by the simulation. Both the data and simulation show the peak of the Fourier spectrum

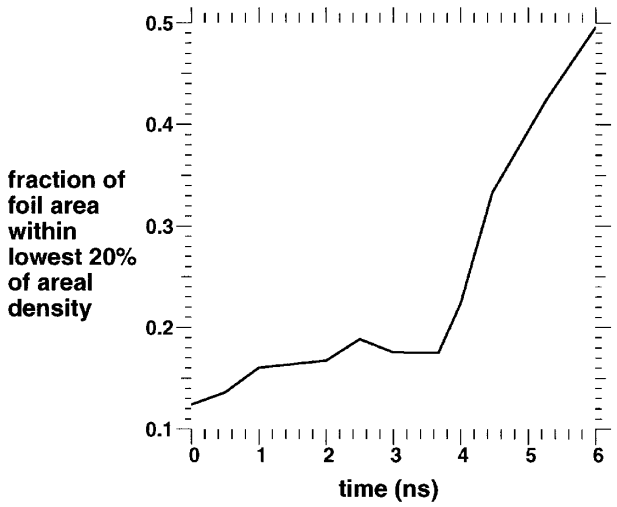

FIG. 3. Fraction of simulated foil area which falls in the lowest 20% of the instantaneous range of areal densities.

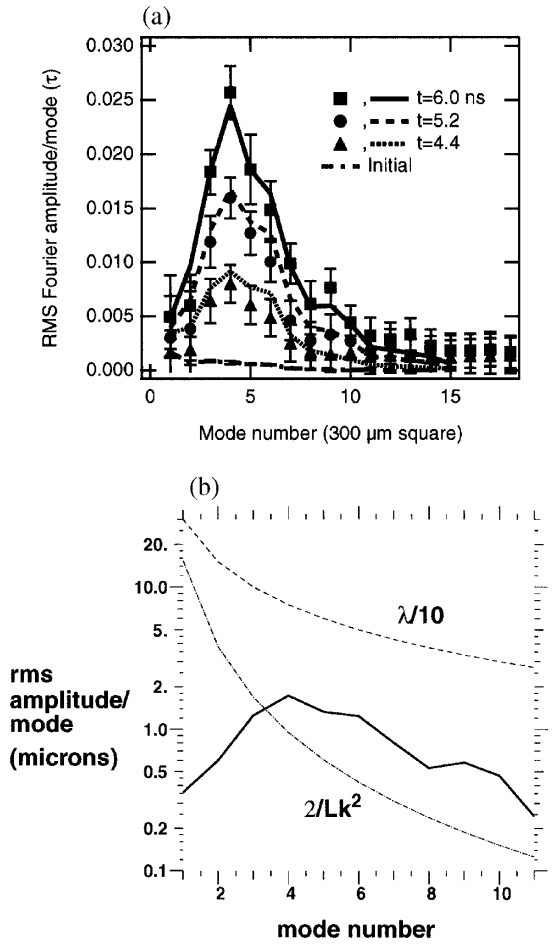

FIG. 4. (a) Fourier spectra of ln(exposure) vs time. The curves are from the HYDRA simulation and include the effect of finite instrumental resolution. The symbols are obtained from the radiograph. (b) Solid curve shows the mode amplitude spectrum obtained from the simulation at 6 ns. Dashed curve is 10% of the wavelength. The dash-dotted curve is the modal saturation amplitude specified by the saturation model $S_{(k)} = 2/Lk^2$.

has developed at mode 4, slightly below the peak of the growth factor spectrum. For the higher modes the experimental error bars are dominated by the white noise present in the radiograph.

Estimates of the rms amplitudes of multimode perturbations in the weakly nonlinear regime are often obtained from the Haan nonlinear saturation model [33]. In the model the bubble side rms amplitude is derived from a quadrature sum of all the individual modes. The amplitude of a particular mode is taken from linear regime evolution until it attains its saturation amplitude $S_{(k)} = \nu/Lk^2$. Here L is the fundamental wavelength, which is related to the density of modes. The saturation parameter ν was originally taken as 4, but more recent simulations indicate $\nu = 2$ is a better fit [29,30,34]. A comparison with the HYDRA simulation indicates that the saturation model with $\nu = 2$ estimates well the time of onset of nonlinear saturation, when the bubble side rms begins to fall below the linear analysis result. Perturbation amplitudes obtained from the simulation exceed $S_{(k)}$ over a broad range by 6 ns, but are much less than $\lambda_n/10$, as shown in Fig. 4(b). Thus the collective nonlinearity observed in the experiment, evidenced by the broad bubbles, is occurring for individual mode amplitudes much smaller than 10% of the wavelength, the threshold for nonlinear saturation of a single mode. The physical amplitudes of the dominant features are determined by the sum of strongly interacting modes with similar wave vectors. Nonlinear saturation occurs when their collective amplitude approaches the characteristic wavelength.

In conclusion, we have described in-flight measurements of a plastic target having a prescribed 3D multimode surface perturbation. This perturbation, which included the range of modes predicted to be most dangerous for our ignition capsules, seeded instabilities which grew into the weakly nonlinear regime. These evolved into round, closely packed bubbles separated by narrow, interconnecting spike sheets. The resulting topology retained a correspondence with the initial perturbation pattern. Simulations with HYDRA matched well the shapes and amplitudes of the bubble and spike structures in the radiograph and were in quantitative agreement with the evolution of the Fourier mode spectra. The experiment and simulation demonstrated that collective nonlinearity occurs in the multimode target when individual mode amplitudes are close to values from a saturation model, much less than the saturation amplitude for a single mode.

We wish to thank T. Shepard for his assistance with hohlraum simulations, and S. V. Weber and D. Ryutov for helpful discussions. We acknowledge the support of the technical staff at Nova. This work was performed under the auspices of the U.S. DOE by the Lawrence Livermore National Laboratory under Contract No. W-7405-ENG-48.

[1] J. D. Lindl and W. C. Mead, Phys. Rev. Lett. **34**, 1273 (1975).
[2] B. A. Hammel *et al.*, J. Quant. Spectrosc. Radiat. Transfer **51**, 113 (1994); Rev. Sci. Instrum. **63**, 5017 (1992).
[3] C. P. Verdon *et al.*, Phys. Fluids **25**, 1653 (1982).
[4] S. E. Bodner, Phys. Rev. Lett. **33**, 761 (1974).
[5] B. A. Remington *et al.*, Phys. Rev. Lett. **67**, 3259 (1991).
[6] B. A. Remington *et al.*, Phys. Fluids **4**, 967 (1992).
[7] B. A. Remington *et al.*, Phys. Fluids B **5**, 2589 (1993).
[8] S. V. Weber *et al.*, Phys. Plasmas **1**, 3652 (1994).
[9] B. A. Remington *et al.*, Phys. Plasmas **2**, 241 (1995).
[10] G. Tryggvason and S. O. Unverdi, Phys. Fluids A **2**, 656 (1990).
[11] T. Yabe, H. Hoshino, and T. Tsuchiya, Phys. Rev. A **44**, 2756 (1991).
[12] H. Sakagami and K. Nishihara, Phys. Rev. Lett. **65**, 432 (1990).
[13] R. P. J. Town and A. R. Bell, Phys. Rev. Lett. **67**, 1863 (1991).
[14] J. P. Dahlburg and J. H. Gardner, Phys. Rev. A **41**, 5695 (1990).
[15] J. P. Dahlburg *et al.*, Phys. Fluids B **5**, 571 (1993).
[16] J. Hecht, U. Alon, and D. Shvarts, Phys. Fluids **6**, 12 (1994); J. Hecht *et al.*, Laser Part. Beams **13**, 423 (1995); D. Shvarts *et al.*, Phys. Plasmas **2**, 2465 (1995).
[17] D. Layzer, Astrophys. J. **122**, 1 (1955).
[18] M. M. Marinak, B. A. Remington, S. V. Weber, R. E. Tipton, S. W. Haan, K. S. Budil, O. L. Landen, J. D. Kilkenny, and R. Wallace, Phys. Rev. Lett. **75**, 3677 (1995).
[19] R. J. Taylor, J. P. Dahlburg, A. Iwase, J. J. Gardner, D. E. Fyfe, and O. Willi, Phys. Rev. Lett. **76**, 1643 (1996).
[20] J. D. Kilkenny, Rev. Sci. Instrum. **63**, 4688 (1992).
[21] K. S. Budil *et al.*, Rev. Sci. Instrum. **67**, 485 (1996).
[22] E. M. Campbell, Laser Part. Beams **9**, 209 (1991).
[23] G. B. Zimmerman and W. L. Kruer, Comments Plasma Phys. Control. Fusion **2**, 51 (1975).
[24] R. L. Kauffman *et al.*, Phys. Rev. Lett. **73**, 2320 (1994).
[25] M. M. Marinak, R. E. Tipton, O. L. Landen, T. J. Murphy, P. Amendt, S. W. Haan, S. P. Hatchett, C. J. Keane, R. McEachern, and R. Wallace, Phys. Plasmas **3**, 2070 (1996).
[26] A. Bar-Shalom *et al.*, Phys. Rev. A **40**, 3183 (1989).
[27] R. M. More, K. H. Warren, D. A. Young, and G. B. Zimmerman, Phys. Fluid **31**, 3059 (1988).
[28] R. J. Wallace, R. L. McEachern, and W. W. Wilcox, ICF Quarterly Report **4**, 79 (1994); Report No. UCRL-LR-105821-94-3.
[29] J. P. Dahlburg, D. E. Fyfe, J. H. Gardner, S. W. Haan, S. E. Bodner, and G. D. Doolen, Phys. Plasmas **2**, 2453 (1995).
[30] M. M. Marinak *et al.*, in ICF Quarterly Report **5**, (1995); Report No. UCRL-LR-105821-95-3.
[31] J. Hecht, D. Ofer, U. Alon, D. Shvarts, S. A. Orszag, and R. L. McCrory, Laser Part. Beams **13**, 423 (1995).
[32] S. W. Haan, Phys. Rev. A **39**, 5812 (1989).
[33] S. W. Haan, Phys. Fluids B **3**, 2349 (1991).
[34] M. J. Dunning and S. W. Haan, Phys. Plasmas **2**, 1669 (1995).